

Smoothing in linear multicompartment biological processes subject to stochastic input

Alexander P Browning¹, Adrienne L Jenner², Ruth E Baker¹, and Philip K Maini¹

¹*Mathematical Institute, University of Oxford, Oxford, United Kingdom*

²*School of Mathematical Sciences, Queensland University of Technology, Brisbane, Australia*

May 17, 2023

Abstract

Many physical and biological systems rely on the progression of material through multiple independent stages. In viral replication, for example, virions enter a cell to undergo a complex process comprising several disparate stages before the eventual accumulation and release of replicated virions. While such systems may have some control over the internal dynamics that make up this progression, a challenge for many is to regulate behaviour under what are often highly variable external environments acting as system inputs. In this work, we study a simple analogue of this problem through a linear multicompartment model subject to a stochastic input in the form of a mean-reverting Ornstein-Uhlenbeck process, a type of Gaussian process. By expressing the system as a multidimensional Gaussian process, we derive several closed-form analytical results relating to the covariances and autocorrelations of the system, quantifying the smoothing effect discrete compartments afford multicompartment systems. Semi-analytical results demonstrate that feedback and feedforward loops can enhance system robustness, and simulation results probe the intractable problem of the first passage time distribution, which has specific relevance to eventual cell lysis in the viral replication cycle. Finally, we demonstrate that the smoothing seen in the process is a consequence of the discreteness of the system, and does not manifest in an equivalent continuum limit description. While we make progress through analysis of a simple linear problem, many of our insights are applicable more generally, and our work enables future analysis into multicompartment processes subject to stochastic inputs.

Keywords

multicompartment, Ornstein-Uhlenbeck, smoothing, robustness, cell lysis, virus life cycle

¹Corresponding author: browning@maths.ox.ac.uk

1 Introduction

Many biological processes comprise multiple independent stages. Viral replication, for example, is a multistage process whereby virions enter a cell through endocytosis, are unpackaged before DNA replication, repackaging, and release (fig. 1a) [1–3]. Similar multistage processes are evident in bacteriophage replication [4] and progression through the cell cycle [5], pervasive at the molecular (i.e., cascade reactions [6]) and macroscopic (i.e., transport through discrete layers [7]) levels, and even manifest in social processes such as queuing [8]. A challenge for many systems is to modulate the impact of what are often highly variable external environments. For instance, while the intermediate stages of viral replication may be optimised to achieve high levels of virion multiplication, the system has either no, or only very limited, control over the number of virions entering the cell [9,10]. For lytic viruses, should the number of virions present inside a cell exceed capacity the cell will lyse, destroying the system and ceasing replication [11].

The time until cell lysis—more broadly, the time until the first occurrence of any event within a stochastic process—can be modelled as a *first passage time* (FPT) problem and is dependent, among many other factors, on the variability and the autocorrelation of the process [12,13]. Statistics such as the variance, autocorrelation, and FPT, are commonly studied in scalar stochastic systems in biology [12,14]. Many linear and non-linear systems described by continuous or discrete-space random walks have closed form solutions available for the aforementioned statistics, and if not for the FPT distribution itself, then for the mean, variance, and higher order moments of the FPT [12,15,16]. Analysis of higher-dimensional systems (i.e., described by more than one first order differential equation‘w) has, to date, been restricted to a fixed number of dimensions; most commonly two or three, where the velocity or acceleration of a particle is described by a stochastic process [17,18]. General techniques for analysis, such

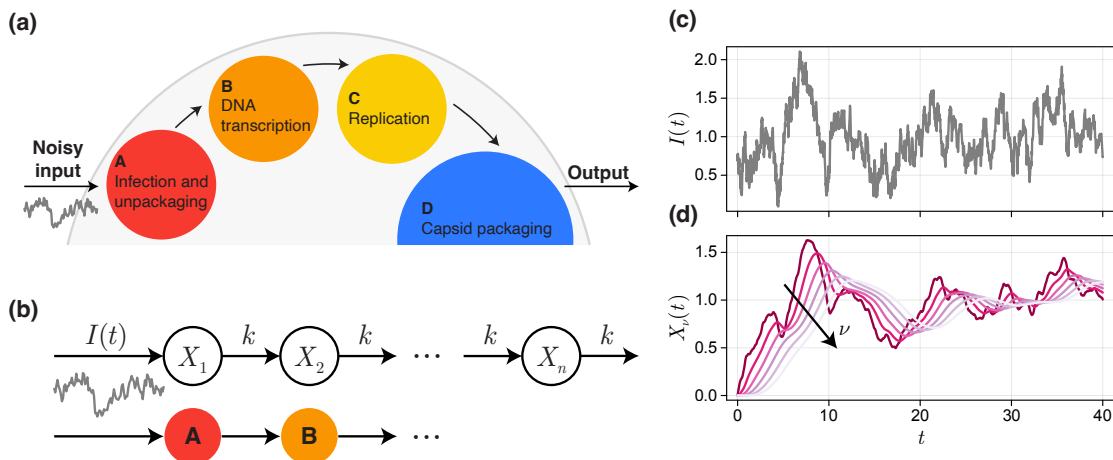


Figure 1. (a) The general viral replication cycle. Virions enter a cell and progress through a multistage process, before accumulating following repackaging. (b) We study a linear analogue of the virus problem, namely a system subject to random input, $I(t)$, modelled as an Ornstein-Uhlenbeck process with mean μ , reversion strength θ , and noise magnitude σ . A realisation of the input is shown in (c). Material then progresses through n compartments at constant rate k . (d) A realisation of the system in (b), where $X_\nu(t)$ models the concentration of material in each compartment $\nu = 1, 2, \dots, 6$. It is evident that passage through the compartments has a smoothing effect.

as through the Fokker-Planck equation, quickly suffer from the curse of dimensionality, and dimension reduction techniques may yield lower-dimensional stochastic processes that lack the Markov property typically exploited in analysis.

Motivated in particular by the viral replication cycle, in this work we study the properties of a linear n -compartment model subject to an independent external input, which we model using a mean-reverting Ornstein-Uhlenbeck process (fig. 1b). Given that, to the best of our knowledge, little is understood about the smoothing effects of multi-compartment processes in general, we study a linear analogue of the viral problem that allows us to formulate a series of analytical expressions for key statistics including the variance, covariance, and autocorrelation function for a general number of compartments, and the rate at which the mean FPT scales with compartment number. We then apply our linear model to study how the behaviour or robustness biological systems can be modified through perturbations to unidirectional progression through the system. Viral replication, for example, is known to be a highly stochastic process, and progression through replication stages is very often not unidirectional [2].

2 Mathematical model

The problem presented in fig. 1b can be expressed as the linear system of stochastic and ordinary differential equations

$$\begin{aligned} dI(t) &= -\theta(I(t) - \mu) dt + \sigma dW(t), \\ dX_1(t) &= (I(t) - kX_1(t)) dt, \\ dX_\nu(t) &= (kX_{\nu-1}(t) - kX_\nu(t)) dt, \quad \nu = 2, \dots, n. \end{aligned} \tag{1}$$

Here, all parameters are real and positive, and $W(t)$ represents a Wiener process such that $W(t + \eta) - W(t)$ is normally distributed with mean zero and variance η .

More compactly, we write

$$d\mathbf{X}(t) = -\mathbf{\Theta}(\mathbf{X}(t) - \boldsymbol{\mu}) dt + \mathbf{S} d\mathbf{W}(t), \tag{2}$$

where we define

$$\mathbf{\Theta} = \begin{pmatrix} \theta & 0 & 0 & \cdots & 0 \\ -1 & k & 0 & \cdots & 0 \\ 0 & -k & k & \cdots & 0 \\ \vdots & & & \ddots & \\ 0 & 0 & 0 & \cdots & k \end{pmatrix}, \quad \boldsymbol{\mu} = \mu \begin{pmatrix} 1 \\ \mathbf{\Theta}_{22}^{-1} \mathbf{e}_1 \end{pmatrix}, \quad \mathbf{S} = \begin{pmatrix} \sigma & \mathbf{0} \\ \mathbf{0} & \mathbf{0} \end{pmatrix}, \tag{3}$$

for $\mathbf{X}(t) = [I(t), X_1(t), \dots, X_n(t)]^\top$. For notational convenience, we interchangeably refer to $I(t)$ as $X_0(t)$ (i.e., the input is thought of as compartment $\nu = 0$). Equation (2) demonstrates that the system is a multidimensional Ornstein-Uhlenbeck process and, therefore, a Gaussian process. We refer to $\mathbf{\Theta}$ as the *connectivity matrix*, as it plays a role similar to that in graph and network theory, defining the connectivity between compartments in the system. Therefore, provided

the system remains linear, we can arbitrarily express systems with any network structure (i.e., with non-local feedbacks or multiply-connected components) using eq. (2). The form of $\boldsymbol{\mu}$, which contains the lower block matrix Θ_{22} corresponding to Θ with the first row and column excluded, simplifies for the system in fig. 1 and eq. (1) to $[\mu, \mu/k, \dots, \mu/k]^\top$. Unless otherwise stated, we fix $\theta = \mu = k = 1$ and $\sigma = 0.5$ as default parameter values when producing simulation results.

There are various initial conditions that we consider in this work, based on the assumption that a stationary limiting distribution for $\mathbf{X}(t)$ exists (since $\theta, k > 0$, this is always true for the form of Θ expressed above, and more generally provided that all the eigenvalues of Θ are negative [19]). The first relevant initial condition is where \mathbf{X}_0 is entirely specified. We refer to this choice as the *fixed* initial condition. For the virus-cell lysis problem, we may be interested in setting $\mathbf{X}_0 = [\mu, 0, \dots, 0]^\top$; i.e., the concentration is zero in all compartments, and the input is initiated at its mean. A second, more biologically realistic initial condition, is where all compartments are initiated with zero concentration, but where the input is initiated from its stationary distribution $I(0) \sim \mathcal{N}(\mu, \sigma^2/(2\theta))$. We refer to this as the *partially-fixed* initial condition. The final initial condition, of interest given that it greatly simplifies some of the analysis, is where all compartments are initiated from the joint stationary distribution for the system. We refer to this as the *stationary* initial condition and the system as a whole in this case as the *stationary system*.

3 Results and Discussion

3.1 Preliminaries

The multivariate Ornstein-Uhlenbeck process conditioned on the initial condition \mathbf{X}_0 has exact solution [19, 20]

$$\mathbf{X}(t)|\mathbf{X}_0 \sim \mathcal{N}(\mathbf{m}(t), \boldsymbol{\Sigma}(t)), \quad (4)$$

where

$$\mathbf{m}(t) = \boldsymbol{\mu} + e^{-\Theta t}(\mathbf{X}_0 - \boldsymbol{\mu}), \quad (5a)$$

$$\text{vec}(\boldsymbol{\Sigma}(t)) = \sigma^2(\Theta \oplus \Theta)^{-1} \left(\mathbf{I} - e^{-(\Theta \oplus \Theta)t} \right) \mathbf{e}_1, \quad (5b)$$

and where \oplus is the Kronecker sum. It follows directly that the stationary distribution, should it exist, is given by

$$\lim_{t \rightarrow \infty} \mathbf{X}(t) \sim \mathcal{N}(\boldsymbol{\mu}, \boldsymbol{\Sigma}_\infty) \quad \text{and} \quad \text{vec}(\boldsymbol{\Sigma}_\infty) = \sigma^2(\Theta \oplus \Theta)^{-1} \mathbf{e}_1. \quad (6)$$

We highlight that the non-stationary covariance matrix (eq. (5b)) does not depend on the initial condition \mathbf{X}_0 and that the mean $\mathbf{m}(t)$ is an affine transformation of the initial condition \mathbf{X}_0 . Therefore, for $\mathbf{X}_0 \sim \mathcal{N}(\mathbf{m}_0, \boldsymbol{\Sigma}_0)$, we have that

$$\mathbf{X}(t) \sim \mathcal{N} \left(\boldsymbol{\mu} + e^{-\Theta t}(\mathbf{m}_0 - \boldsymbol{\mu}), \boldsymbol{\Sigma}(t) + e^{-\Theta t} \boldsymbol{\Sigma}_0 e^{-\Theta^\top t} \right). \quad (7)$$

This expression reduces to the fixed initial condition for $\mathbf{\Sigma}_0 = \mathbf{0}$, to the semi-fixed initial condition for $\mathbf{\Sigma}_0 = \text{diag}(\sigma^2/(2\theta), 0, \dots, 0)$, and to the stationary initial condition for $\mathbf{\Sigma}_0 = \mathbf{\Sigma}_\infty$.

The final result for the multivariate Ornstein-Uhlenbeck process that is relevant is the joint distribution of $\mathbf{X}_{t_1, t_2, \dots} = [\mathbf{X}(t_1), \mathbf{X}(t_2), \dots]^\top$, which is multivariate normal with covariance matrix

$$\mathbf{\Sigma}_{t_1, t_2, \dots} = \begin{pmatrix} \mathbf{\Sigma}(t_1) & \mathbf{\Sigma}(t_1)e^{-\mathbf{\Theta}^\top(t_2-t_1)} & \mathbf{\Sigma}(t_1)e^{-\mathbf{\Theta}^\top(t_3-t_1)} & \dots \\ e^{-\mathbf{\Theta}(t_2-t_1)}\mathbf{\Sigma}(t_1) & \mathbf{\Sigma}(t_2) & \mathbf{\Sigma}(t_2)e^{-\mathbf{\Theta}^\top(t_3-t_2)} & \dots \\ & \vdots & & \ddots \end{pmatrix}. \quad (8)$$

If $t_1, t_2, \dots \gg 0$ such that $\mathbf{\Sigma}(t_i) = \mathbf{\Sigma}_\infty$, then eq. (8) corresponds to the joint stationary distribution of $\mathbf{X}_{t_1, t_2, \dots}$ and, along with $\mathbb{E}(\mathbf{X}(t_i)) = \boldsymbol{\mu}$, fully defines the system as a stationary Gaussian process. Furthermore, we can derive the distribution for all initial conditions (i.e., eqs. (5b), (6) and (7)) from the joint stationary distribution from marginalising or conditioning the joint stationary distribution accordingly (this is straightforward for the multivariate normal distribution, see [21]).

3.2 Quantifying smoothing in linear multicompartment processes

The structure of \mathbf{S} , whereby noise enters the system only through the first compartment independently of other compartments, results in a simpler form of the stationary covariance matrix, given by eq. (6) and which we now denote simply by $\mathbf{\Sigma}_\infty$, compared to the standard multivariate Ornstein-Uhlenbeck process. In particular, $\mathbf{\Sigma}_\infty$ depends only upon the first column of $(\mathbf{\Theta} \oplus \mathbf{\Theta})^{-1}$. In the supporting material, we provide a full derivation for analytical expressions for $\mathbf{\Sigma}_\infty$ in two cases: the first where $\theta = k$, and the second where both θ and k are allowed to vary freely. In this section, we summarise and discuss the main results.

For $\theta = k$, elements of the symmetric matrix $\mathbf{\Sigma}_\infty$ are given by the recurrence relation

$$\mathbf{\Sigma}_\infty^{(i,j)} = \frac{\mathbf{\Sigma}_\infty^{(i,j-1)} + \mathbf{\Sigma}_\infty^{(i-1,j)}}{2}, \quad i, j = 2, 3, \dots \quad (9)$$

subject to the boundary conditions

$$\mathbf{\Sigma}_\infty^{(1,1)} = \frac{\sigma^2}{2\theta} \quad \text{and} \quad \mathbf{\Sigma}_\infty^{(1,i)} = \frac{\mathbf{\Sigma}_\infty^{(1,i-1)}}{1+\theta}, \quad i = 1, 2, \dots \quad (10)$$

The recurrence relation yields

$$\mathbf{\Sigma}_\infty^{(i,j)} = \frac{\sigma^2 \Gamma(i+j-1)}{2^{i+j-1} \Gamma(i) \Gamma(j) \theta^3}, \quad (11)$$

for covariances relating to the compartments themselves (i.e., $i, j = 2, 3, \dots$). Thus, the stationary variance of compartment $\nu \geq 1$ is given by

$$\sigma_\nu^2 = \mathbf{\Sigma}_\infty^{(\nu+1, \nu+1)} \sim \frac{\sigma^2}{2\theta^3 \sqrt{\nu\pi}}, \quad (12)$$

where we have applied Stirling's approximation [22] to derive an asymptotic expression for the

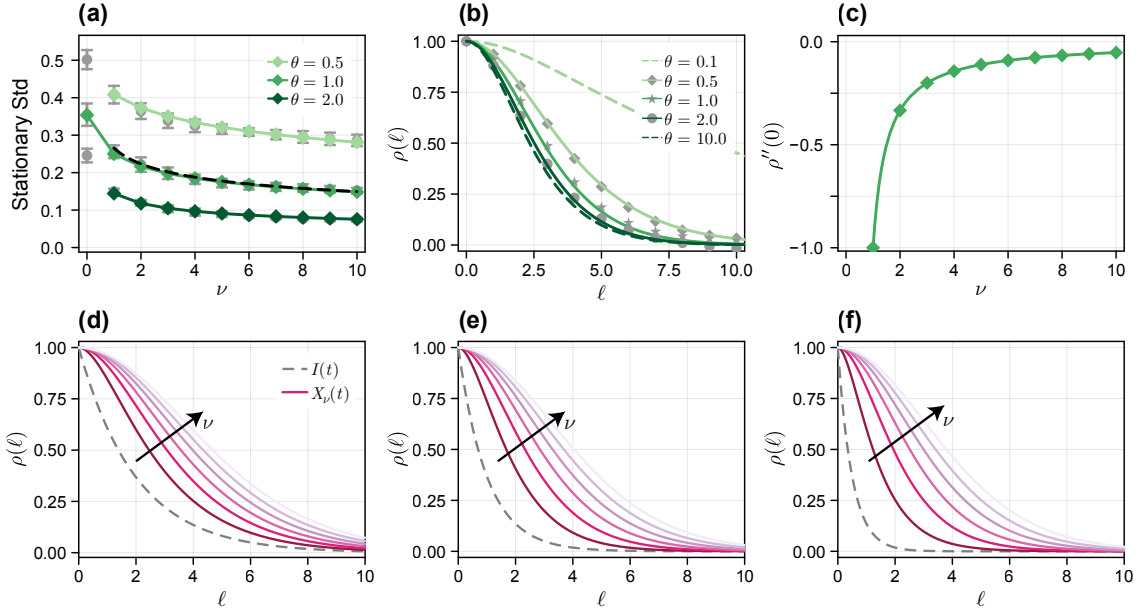


Figure 2. (a) Stationary standard deviation as a function of compartment number (compartment $\nu = 0$ refers to $I(t)$). Shown are mean \pm std from numerical simulations constructed from 10 replicates of 100 simulations (grey), and the corresponding analytical solution (colour). (b) Simulated and analytical ACFs for compartment $\nu = 3$. (c) Second derivative of the ACF at $\ell = 0$ for $\theta = k = 1$ calculated directly from eq. (15) (diamonds), and using the analytical expression in eq. (16) (solid). (d–f) Analytical ACFs for $I(t)$ (grey dashed) and $X_\nu(t)$ (colour of increasing brightness for $\nu = 1, 2, \dots, 6$). Unless otherwise stated, the other parameters are fixed at $\theta = \mu = k = 1$, and $\sigma = 0.5$.

large compartment number, $\nu \gg 1$, limit. In fig. 2a, we compare both the exact and asymptotic expressions for the stationary variance to a numerical approximation produced through repeated simulation of the SDE. Even for $\nu = 1$, the asymptotic expression produces excellent agreement with simulation results.

Relaxing the restriction that $\theta = k$ yields a closed form solution for Σ_∞ , which simplifies along the diagonal to yield

$$\sigma_\nu^2 = \frac{\sigma^2}{k^2 \theta (1 - (\theta/k)^2)^\nu} \frac{B\left(\frac{1-\theta/k}{2}, \nu, \nu\right)}{B(\nu, \nu)}, \quad (13)$$

where $B(\cdot, \cdot)$ and $B(\cdot, \cdot, \cdot)$ refer to the Beta function and incomplete Beta function, respectively. We show both analytical and simulation results for σ_ν^2 in this more general case in fig. 2a.

Taken all together, the results in fig. 2a show that the variance dissipates as the compartment number increases. However, this happens relatively slowly: the analytical expression for $\theta = k$ provides a rate of decay of order $\nu^{-1/2}$. Importantly, the expression in eq. (12) indicates that the variance does, indeed, tend to zero as $\nu \rightarrow \infty$. To the best of our knowledge it is not possible to derive a similar expression for general θ , however we provide in the supplementary material a simple proof that $\sigma_{\nu+1}^2 < \sigma_\nu^2$ for $\theta > 0$ to show that the variance is a strictly decreasing function and tends to zero for large compartment numbers. From this, we also gain insight into the asymptotic behaviour of the solution for small or large θ . As $\theta \rightarrow \infty$, $\sigma_0^2 \rightarrow 0$, and so the system becomes fully deterministic. In the problem itself, this represents a large mean reversion

strength, so that effectively $I(t) \equiv \mu \forall t$. For $\theta = 0$, the input function becomes purely Brownian motion and the stationary solution does not exist.

While compartment variances and covariances are statistics relating to the process at a single time point, the autocorrelation function (ACF) provides insight into how smooth the resultant time-series is. By deriving an analytical expression for $e^{-\Theta}$, we can obtain an analytical expression for the autocorrelation function (ACF). While this is relatively straightforward for the $\theta = k$ case, it is, however, significantly more involved in the more general case, for which the expression obtained is no more helpful than the analytical expression for the autocorrelation function involving the calculation of $e^{-\Theta}$ directly (supplementary material). For $\theta = k$ we obtain

$$\rho_\nu(\ell) := \text{corr}(X_t^{(\nu)}, X_{t+\ell}^{(\nu)}) = e^{-k\ell} {}_1F_1(-\nu, -2\nu, 2k\ell), \quad (14)$$

where ${}_1F_1(\dots)$ is the confluent hypergeometric function. Equation (15) can be expressed as

$$\rho_\nu(\ell) = e^{-k\ell} \left(1 + k\ell + \sum_{i=2}^{\nu} c_{i,\nu} (k\ell)^i \right), \quad (15)$$

where coefficients $c_{i,\nu}$ depend on i and ν , which yields a simple expression for $\nu = 1$. We also obtain the scaling of the autocorrelation as a function of ν by calculating the curvature of the ACF at $\ell = 0$,

$$\rho_\nu''(0) = \frac{k^2}{1 - 2\nu}, \quad (16)$$

where $'$ indicates a derivative with respect to the lag, ℓ . In fig. 2b, we compare analytical expressions for the ACF to those obtained through simulation, and in fig. 2d–f we show the ACF for the system in fig. 1 for $\theta = 0.5, 1$ and 2 . In fig. 2c we compare the analytical expression for the ACF curvature (eq. (16)) to that calculated directly from eq. (15) using numerical methods.

As expected, we see qualitatively from the results in fig. 2 that further compartments remain correlated for longer. Considered alone, the stationary process $X_\nu(t)$ is itself an, albeit non-Markovian, Gaussian process, fully defined by its variance and autocorrelation function. Therefore, should we normalise each compartment by its respective standard deviation, $X_\nu(t)/\sigma_\nu(t)$, the properties of the resultant process are encoded entirely in the ACF. Given the system in eq. (1), we expect $X_\nu(t)$ to be ν -times differentiable (the input, $I(t) = X_0(t)$ is nowhere differentiable) and therefore expect that further compartments will be smoother. For $\nu \geq 1$, we can see such smoothing directly from the ACF curvature in eq. (16). For a small increment, $\ell \ll 1$, we have that $\rho_\nu(\ell) \sim 1 + (\rho_\nu''(0)/2)\ell^2$ and therefore $\rho_{\nu_1}(\ell) \sim \rho_{\nu_2}(\omega_{\nu_1,\nu_2}\ell)$ where

$$\omega_{\nu_1,\nu_2} = \sqrt{\frac{\rho_{\nu_2}''(0)}{\rho_{\nu_1}''(0)}} = \sqrt{\frac{1 - 2\nu_1}{1 - 2\nu_2}}, \quad (17)$$

gives the dilation factor. Should we take $\nu_1 = 1$, then $X_\nu(t)$ varies a factor of $\omega_{1,\nu} = \sqrt{2\nu - 1}$ more slowly than $X_1(t)$.

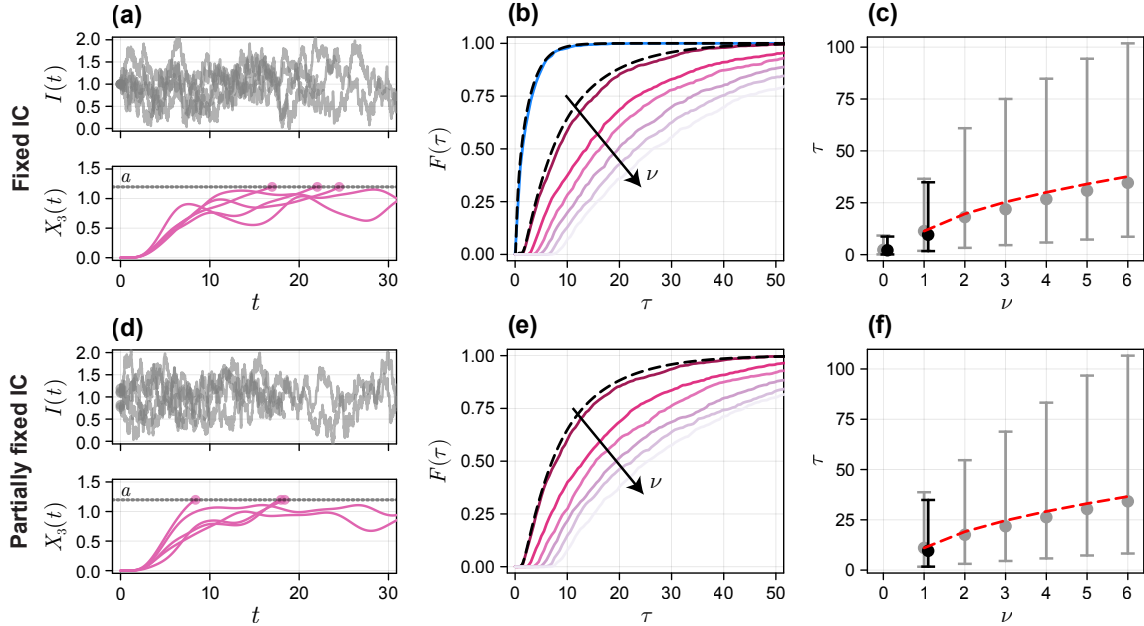


Figure 3. (a,d) Realisations of a three compartment system initiated using (a) the fixed initial condition and (d) the partially-fixed initial condition. Solutions are terminated at $t = \tau : X_3(\tau) > a$, yielding τ as the FPT. (b,e) Distribution function for the FPT constructed from (colour) 1000 realisations of the SDE and (dashed black) a finite difference solution to eq. (18). (c,f) Mean, 2.5% quantile, and 97.5% quantile for the FPT distribution constructed from (grey) 1000 realisations of the SDE and (black) a finite difference solution to eq. (18). Shown in red-dashed is an approximation to the mean FPT constructed by scaling the FPT for $\nu = 1$ based on matching the second-derivative of the autocorrelation function (eq. (16)). The barrier for each compartment is located at $a = \tilde{a}\sigma_\nu$ where $\tilde{a} = 1$. Other parameters are fixed at $\theta = \mu = k = 1$, and $\sigma = 0.5$.

3.3 First passage time (FPT)

Motivated by the viral replication problem, we are now interested in studying the FPT distribution of individual compartments. That is, the time at which $X_\nu(t)$ first crosses the threshold value $X_\nu(t) = a$ from below, for $a > X_\nu(0)$. To effectively compare FPT distributions between compartments, we scale the threshold by the associated stationary standard deviation of the relevant compartment such that $a = \mu + \tilde{a}\sigma_\nu$, where σ_ν is given by eq. (12) and \tilde{a} is specified. Formally, we define the FPT by $\tau = \inf\{t : X_\nu(t) \geq a\}$ and its associated probability density and distribution functions by $f(\tau)$ and $F(\tau)$, respectively. We focus on fixed and partially-fixed initial conditions where we ensure that $X_\nu(0) < a$, demonstrated in fig. 3a,d, respectively, for $\nu = 3$ and $\tilde{a} = 1$.

It is not generally possible to derive an analytical expression for $f(t)$, nor to formulate a closed-form integral equation that can be solved numerically. The only general way to solve for $f(t)$ is through a numerical solution to the Fokker-Planck equation, a $\nu + 1$ dimensional partial differential equation. However, following the procedure for Markovian Gaussian processes [17,18] we are able to formulate a reasonable approximation for $\nu = 1$, although we revert to simulating the FPT for the more general case.

Denote by $p_\nu(x, t)$ the density of the random variable $X_\nu(t)$, and by $p_\nu(x, t, \tau)$ the joint

density with the first passage time. By marginalising $p_\nu(x, t, \tau)$ with respect to τ we have that

$$p_\nu(a, t) = \int_0^\infty p_\nu(a, t, \tau) d\tau = \int_0^t K(t, \tau) f(\tau) d\tau, \quad (18)$$

where $K(t, \tau) = p_\nu(a, t|\tau)$ is the density of $X(t)$ given the first passage time τ . The upper limit of t in the second integral arises since $p_\nu(a, t|\tau) = 0$ for all $t < \tau$; in other words, should a passage not have occurred by time t , then $X_\nu(t) < a$ and so the particle cannot be at location $X_\nu(t) = a$. Equation (18) is a Volterra equation of the first kind and, while generally difficult, can be solved numerically provided $K(t, \tau)$ can be computed. As $I(t) = X_0(t)$ is Markovian, $p_0(a, t|\tau) = p_0(a, t|a, \tau)$ is readily available and for certain parameter combinations, eq. (18) can be solved analytically to give the FPT density of the Ornstein-Uhlenbeck process [23, 24].

For $\nu > 0$ the conditional probability $p_\nu(a, t|\tau)$ cannot be calculated exactly; further we find that the standard approach of approximating $p_\nu(a, t|\tau) \approx p_\nu(a, t|a, \tau)$ provides relatively poor results. To obtain a more accurate approximation, we note that the full state process $\mathbf{X}(t)$ is Markovian, and that $X_\nu(s) = a$ and $X'_\nu(s) > 0$ if and only if s is a passage time. By eq. (1), $X'_\nu(s)$ is a linear combination of other states, and so the random variable $[X_\nu(s), X'_\nu(s)]$ is Markovian with a multivariate normal distribution. Thus, we approximate

$$p_\nu(a, t|\tau) \approx p_\nu(a, t|X(\tau) = a, X'(\tau) > 0). \quad (19)$$

Note that eq. (19) is not exact despite the full state being Markovian as we have not conditioned on a point, but rather the range $X'(\tau) > 0$; while the distribution of $X'(s)$ is normal, the distribution of $X'(\tau)$ is not necessarily so. We find that a numerical solution to eqs. (18) and (19) gives a reasonable approximation to $f(\tau)$ for $\nu = 1$ (fig. 3b).

Results in fig. 3b,e show the FPT distribution function, $F(\tau)$, for both the fully- and partially-fixed initial conditions for $\theta = k = 1$, respectively. The coloured curves are produced from 1000 realisations of the SDE model, and the black curves from a numerical solution to eq. (18). An interpretation of $S(\tau) = 1 - F(\tau)$ is that of the *survival probability*: should a passage indicate system failure, $S(\tau)$ represents the probability that a system is functional at time τ . For the virus-cell lysis problem, we interpret this as the probability that cell lysis has not occurred, and viral production is ongoing. Visual inspection of the results in fig. 3 reveal little difference between both initial conditions, particularly for larger compartment numbers. This observation is unsurprising upon comparison between the magnitude of the mean FPT, $\mathbb{E}(\tau) \sim \mathcal{O}(10)$, and the largest eigenvalue of $-\Theta$, $\lambda = -1$, demonstrating that the influence of the initial condition decays like $\exp(-t)$ (eq. (5a)), much faster than the mean FPT.

The most obvious result from fig. 3b,e, as one might expect from the analysis of compartment smoothing in the previous section, is that the FPT is generally larger for further compartments; accounting for differences in the stationary variance by comparing compartments across the same value of \tilde{a} indicates that further compartments can be thought to be more robust to external noise. Not only does the expected FPT increase (equal to the area under the survival function $S(\tau)$), but so too do the lower quantiles, evidenced by the time taken for the distribution function $F(\tau)$ to visually become non-zero. We investigate these qualitative observations further in fig. 3c,f, by calculating the mean, 2.5% and 97.5% quantiles for the FPT for each compartment.

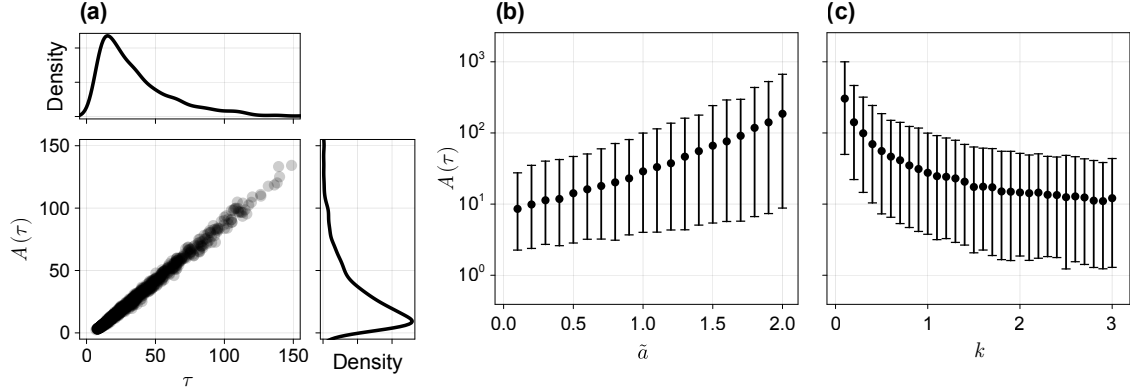


Figure 4. Cumulative production at the first passage time. We investigate the cumulative production at the first passage time, denoted by $A(\tau) = \int_0^\tau k X_6(t) dt$, for a six compartment system. (a) Relationship between τ and $A(\tau)$ based on 1000 replicates of the SDE with $\tilde{a} = k = 1$. We show both a scatter plot of the joint density and kernel density estimates constructed from the marginals. (b,c) Mean, 2.5% quantile, and 97.5% quantile of $A(\tau)$ constructed from 1000 replicates of the SDE as (b) \tilde{a} is varied, and (c) k is varied.

Aside from an overall increase in the FPT, there is a notable increase in the inter-quantile range or variance for larger compartment numbers.

By normalising the location of the threshold, the FPT is almost entirely a function of the ACF for each compartment. The compartment variance still plays a role for the initial conditions considered in fig. 3, as the relative distance between the initial condition $X_\nu(0) = 0$ and the threshold depends on σ_ν . The settling phase, however, occurs relatively quickly: for $k = 1$, the system settles to equilibrium like $\exp(-t)$, much faster than the typical FPT. Thus, the compartment smoothing effect characterised by $\rho_\nu(\ell)$ is the primary factor that drives increases in FPT for further compartments. In fig. 3c,f, we show that the small-lag ACF dilation factor, given analytically by eq. (17), provides an excellent match to numerical results for the mean first passage time, confirming qualitatively that, similarly to the compartment variance, the FPT scales like $\sqrt{\nu}$.

3.4 Production before system failure

While for many systems the FPT, τ , may itself be of primary interest, for others it may be a function of the FPT that is important. For the virus-cell lysis problem, for example, of primary interest may be the total amount of virus produced by the system prior to cell lysis: a viral genotype that maximises per-host-cell virion production may have a fitness advantage over others.

We define cumulative production as the total amount of material to pass out of the system, $A(t) = \int_0^t k X_\nu(t) dt$, and investigate $A(\tau)$ through simulation in fig. 4 for $\nu = 6$ and $\theta = k = 1$. Results in fig. 4a show that $A(\tau)$ is highly correlated with τ . We expect this, as both initial settling and ACF decay occur much faster on average than τ . Thus, for the linear system considered in this work, we hypothesise that a genotype that maximises the expected FPT could be considered equivalent to one that maximises the production prior to lysis.

In fig. 4b,c we perform a parameter sweep to determine the distribution of $A(\tau)$ as a function

of the threshold location, \tilde{a} , and the compartment transfer rate, k . Clearly, for thresholds that are larger, and hence hit less crossed more rarely, we see an increase in $A(\tau)$. We view the threshold location as a feature of the host-system: for the virus-cell lysis problem, this is a biological feature of the host cell, and not a feature of the viral genome. Of direct interest is the relationship between k and $A(\tau)$. The results in fig. 4c show that systems with large compartment transfer rates have lower cumulative production than those that operate slowly. While we cannot interpret the expression for the ACF curvature (eq. (16)) exactly for $\theta \neq k$, the expression does suggest that the ACF curvature is proportional to k^2 , thus increasing the rate at which material travels through the system is detrimental to robustness. In the virus-cell lysis problem, the potential fitness advantage gained by operating slowly (i.e., small k) must be considered alongside the potential immune-escape advantages in operating quickly. Analysis of more complicated, non-linear, compartment processes may also yield non-monotonic relationships between fitness and speed or other parameters; such analysis is, however, beyond the scope of the present work.

3.5 Non-local feedback to alter system robustness

Another way in which systems can potentially increase their robustness to input noise is through non-local feedback or feedforward loops. We now investigate the relative change to the stationary variance and ACF curvature in the final compartment of a system with an additional transfer from compartment n to compartment m of magnitude ε (fig. 5a). A transfer with $m < n$ is considered a feedback, with $m > n$ a feedforward. Since the within system dynamics are deterministic, a transfer with $m = n$ has no net effect on the dynamics.

The results in fig. 5b,c show that the output variance can be reduced, potentially significantly, through a feedback. For the system considered, a feedback from the final to the first compartment has the largest effect, yielding a reduction of over 30% to the stationary standard deviation. In fig. 5d,e we show a similar affect on the curvature of the ACF. Interestingly, feedbacks from the second last compartment to the first compartment, or the last to the second, yield the greatest reduction in the curvature of the ACF. We also observe a non-linear relationship between the magnitude of the feedback and the ACF curvature. For example, a small ($\varepsilon = 0.1$) feedforward rate from the first to the last compartment yields a reduction in the ACF curvature whereas a large ($\varepsilon = 1$) feedforward rate yields an increase in the curvature.

3.6 Continuum limit

While the focus of the present work is on multicompartment processes, a natural extension is to investigate smoothing in processes that occur on a continuum (for example, where compartment number, ν , is a continuous measure of how far a particle has progressed through a system). Therefore, we consider a refinement of the discrete process by dividing each compartment into $1/\Delta$ subcompartments, each of width Δ (fig. 6a). To maintain the effective total time a particle spends in the system, we assume that the subcompartment transfer rate becomes $\hat{k} = k/\Delta$ such

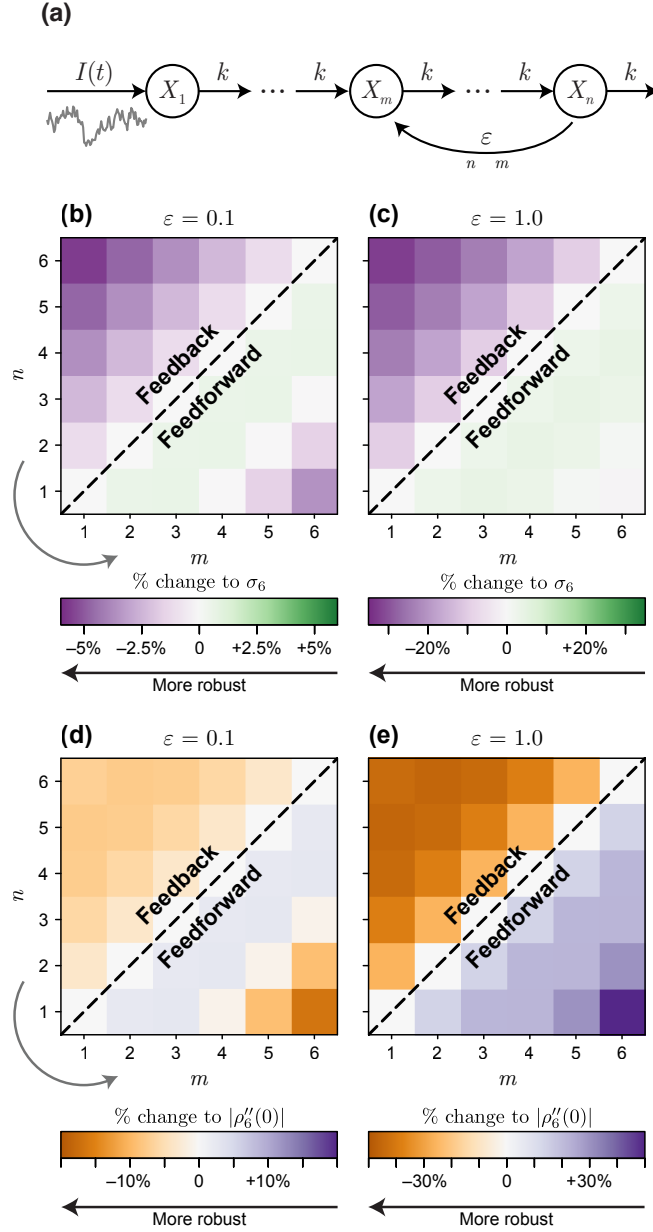


Figure 5. System with non-local feedback. We investigate the effect of a non-local feedback (or feedforward) of magnitude ε from compartment n to compartment m on the stationary standard deviation of $X_6(t)$, denoted σ_6 , and the magnitude of the ACF curvature, denoted $|\rho_6''(0)|$. In all cases, a reduction in each statistic corresponds to a potentially more robust system.

that

$$\begin{aligned} X_0(t) &= I(t), \\ \frac{dX_i}{dt} &= \frac{k}{\Delta}(X_{i-1}(t) - X_i(t)), \quad i > 0, \end{aligned} \quad (20)$$

where $\nu = (i-1)\Delta$. Note that to formulate the input as a boundary condition, we have modified the original system such that the input transfers to the first compartment at rate k (i.e., $X_1(t)$ now experiences an input of $kI(t)$ compared to the input of $I(t)$ in eq. (1)). This formulation is equivalent to the original formulation for $k = 1$.

We denote $x(\nu, t) = X_i(t)$, and take $\Delta \rightarrow 0$ to yield an advection equation with Dirichlet boundary condition

$$\begin{aligned} \frac{\partial x}{\partial t} &= -k \frac{\partial x}{\partial \nu}, \\ x(0, t) &= \begin{cases} I(t), & t > 0, \\ 0, & t \leq 0, \end{cases} \\ x(\nu, 0) &= 0, \quad \nu > 0. \end{aligned} \quad (21)$$

with exact solution

$$x(\nu, t) = I(t - \nu/k). \quad (22)$$

As an advection equation, the continuum analogue of the multicompartment system corresponds to exact (undamped) transport of material through the system. We conclude, therefore, that the smoothing we see is a uniquely discrete effect. This conclusion becomes obvious should each compartment be viewed as a well-mixed segment of “length” Δ in ν -space. Transfer between each compartment represents flow across the left boundary. As the “length” of each

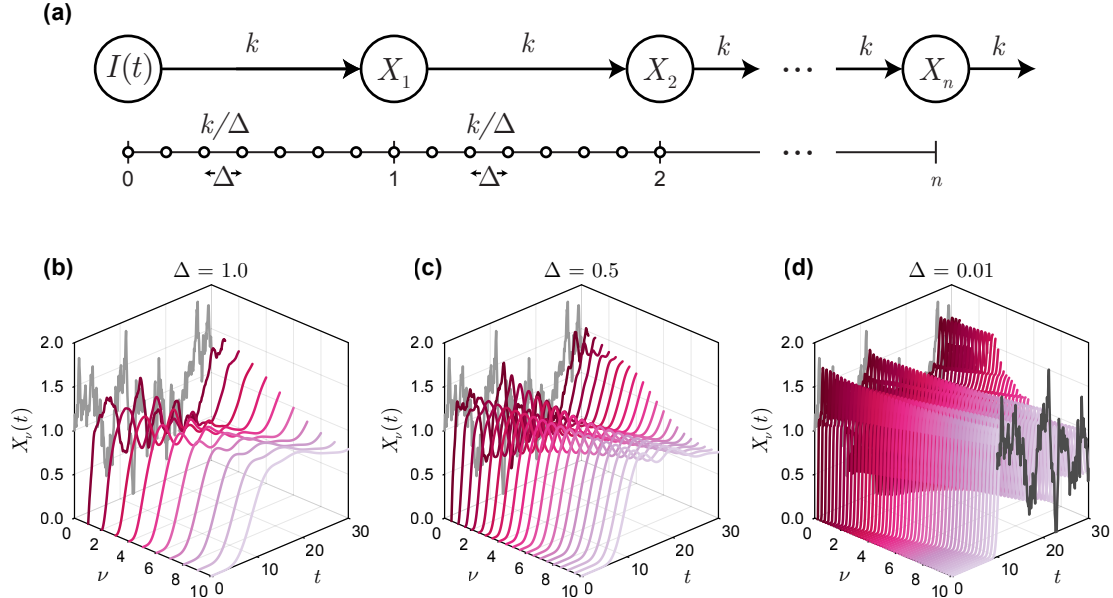


Figure 6. Material transport through a system approaching the continuum limit. (a) Compartments in the discrete system are divided into subcompartments of “length” Δ , while the “transfer density” is kept fixed. (b–d) Solutions of the discrete system for decreasing Δ . All systems are subject to identical input $I(t)$ (grey). In (d), the shifted input $I(t - 10)$ is shown at $\nu = 10$ for comparison with the transported concentrations. Other parameters are fixed $\theta = \mu = k = 1$, and $\sigma = 0.5$.

compartment becomes smaller, the left boundary approaches the right, and thus the finite difference between successive compartments diminishes. Thus, smoothing can be viewed as a consequence of within-compartment mixing, a feature of the discrete system that vanishes as the size of each compartment tends to zero. The same conclusion can be reached by viewing passage through each compartment as a Poisson process, such that the total time particles spend in the system has an Erlang distribution, with variance n/k^2 . The rescaling in the continuum model affects both the total number of compartments $n \mapsto n/\Delta$ and transfer rate $k \mapsto k/\Delta$. While the expected amount of time particles spend in the system remains unchanged, the variance is now given by $\Delta n/k$, which vanishes as $\Delta \rightarrow 0$. Thus, particles are transported deterministically through the system.

We perform a numerical experiment in fig. 6 and simulate three systems subject to an identical input, with identical total length $n = 10$, and with compartment spacing reducing from $\Delta = 1$ to $\Delta = 0.01$. In effect, the solution to the discrete system corresponds exactly to a forward difference approximation to that of the advection equation (eq. (21)). Smoothing in both the autocorrelation and variance is evident in all cases with finite Δ , however, it diminishes significantly for $\Delta = 0.01$. The emergence of the travelling-wave-type solution, given by eq. (21) and where the fixed- ν solution is given by a linear delay, is also evident in fig. 6d, in which we observe a non-zero concentration develop in each compartment after the finite time $t = \nu/k$.

4 Conclusion

Multicompartment processes are ubiquitous in biology; from linear progression through the cell cycle, to phage replication in bacteria and the propagation of viruses by hijacked cellular machinery. Our analysis demonstrates that even a fundamental linear multicompartment structure provides potential advantages and benefits to the systems that employ them. Most notable is the effect of such systems to smooth and provide an additional degree of control over external noise, consequentially increasing resilience and robustness. The inclusion of feedback and feed-forward loops can enhance this effect, providing systems with additional degrees of control and contributing to so-called perfect adaptation [25, 26]. Such loops provide a potential explanation for out-of-order progression in some systems, for example, whereby viral replication does not occur as a unidirectional process [2]. Our work demonstrates that feedback loops could yield a fitness advantage through more favourable statistical properties of viral load compared with perfect progression through the replication cycle. Indirectly, these loops provide systems with the ability to tune the first passage time distribution, potentially yielding an *optimal* lysis time [13, 27]. While we restrict our analysis to a single non-local feedback or feedforward, future work may study more general optimal network structures, subject to constraints informed by a more specific physical or biological problem.

Analysis of a linear model system, subject to Ornstein-Uhlenbeck-type noise, allows us to present closed-form expressions for key statistics, providing a fundamental understanding that would be otherwise unavailable for more complicated systems. We reveal that noise dissipates in systems with unidirectional flow, eventually vanishing in an infinite-compartment system. However, we show that this effect is tied to a finite flow rate: scaling to yield continuous flow through

a continuum limit approximation reveals that smoothing is a discrete effect, caused by *within compartment* mixing. While many simple results are only available for the constant flow rate assumption, arbitrarily connected linear systems yield a multidimensional Ornstein-Uhlenbeck process with statistical properties computable semi-analytically through the exponentiation of a connectivity matrix.

Importantly, we lay the foundation for future work to explore the properties of more general multi-compartment systems subject to external noise. For instance, study of the interaction between the external timescales (i.e., autocorrelation of the external input) and the internal timescales (i.e., progression through the system) is highly relevant to specific biological problems: in the virus-cell lysis problem, this interaction is relevant for immune system detection and, therefore, infection clearance. Aside from external noise, other stochastic features, including both between-cell and between-virion heterogeneity and fluctuations in the replication process itself are known to play an important role in within-host virus replication [3, 10, 28, 29]. Despite these observations, the study of multicompartment problems with the stochastic mathematical models requisite to capture important features is presently scarce, albeit a rich area for both mathematical and biological insight.

Data availability

Code used to produce the results are available on GitHub at <https://github.com/ap-browning/multicompartment>.

Author contributions

All authors conceived the study, provided feedback on drafts, and gave approval for final publication. A.P.B. implemented the computational algorithms and drafted the manuscript.

Acknowledgements

The authors thank Ben Hambly and Hilary Hunt for helpful discussions.

References

- [1] Cann A.J. Replication of viruses. In: Encyclopedia of Virology (Third Edition). Academic Press; 2008. p. 406–412.
- [2] Louten J. Virus Replication. In: Essential Human Virology. Academic Press; 2016. p. 49–70.
- [3] Sazonov I, Grebennikov D, Meyerhans A, Bocharov G. Sensitivity of SARS-CoV-2 life cycle to IFN effects and ACE2 binding unveiled with a stochastic model. *Viruses*. 2022;14(2):403. doi:10.3390/v14020403.
- [4] Campbell A. The future of bacteriophage biology. *Nature Reviews Genetics*. 2003;4(6):471–477. doi:10.1038/nrg1089.
- [5] Morgan D.O. *The Cell Cycle: Principles of Control*. London: New Science Press Ltd; 2007.
- [6] Huang CY, Ferrell JE. Ultrasensitivity in the mitogen-activated protein kinase cascade. *Proceedings of the National Academy of Sciences*. 1996;93(19):10078–10083. doi:10.1073/pnas.93.19.10078.

- [7] Carr EJ, Simpson MJ. New homogenization approaches for stochastic transport through heterogeneous media. *The Journal of Chemical Physics*. 2019;150(4):044104. doi:10.1063/1.5067290.
- [8] Liu L, Liu X, Yao DD. Analysis and optimization of a multistage inventory-queue system. *Management Science*. 2004;50(3):365–380. doi:10.1287/mnsc.1030.0196.
- [9] Schulte MB, Andino R. Single-cell analysis uncovers extensive biological noise in poliovirus replication. *Journal of Virology*. 2014;88(11):6205–6212. doi:10.1128/jvi.03539-13.
- [10] Jones JE, Sage VL, Lakdawala SS. Viral and host heterogeneity and their effects on the viral life cycle. *Nature Reviews Microbiology*. 2021;19(4):272–282. doi:10.1038/s41579-020-00449-9.
- [11] Heaton NS. Revisiting the concept of a cytopathic viral infection. *PLoS Pathogens*. 2017;13(7):e1006409. doi:10.1371/journal.ppat.1006409.
- [12] Redner S. *A Guide To First-Passage Processes*; 2001.
- [13] Kannoly S, Singh A, Dennehy JJ. An optimal lysis time maximizes bacteriophage fitness in quasi-continuous culture. *mBio*. 2022;13(3):e03593–21. doi:10.1128/mbio.03593-21.
- [14] Allen LJS. *An Introduction to Stochastic Processes with Applications to Biology*. Boca Raton, Florida: Chapman & Hall/CRC Press; 2011.
- [15] Simpson MJ, Sharp JA, Baker RE. Survival probability for a diffusive process on a growing domain. *Physical Review E*. 2015;91(4):042701. doi:10.1103/physreve.91.042701.
- [16] Rijal K, Prasad A, Singh A, Das D. Exact distribution of threshold crossing times for protein concentrations: implication for biological timekeeping. *Physical Review Letters*. 2022;128(4):048101. doi:10.1103/physrevlett.128.048101.
- [17] Bernard MC, Shipley JW. The first passage problem for stationary random structural vibration. *Journal of Sound and Vibration*. 1972;24(1):121–132. doi:10.1016/0022-460x(72)90128-9.
- [18] Grigoriu M. First passage times for Gaussian processes by Slepian models. *Probabilistic Engineering Mechanics*. 2020;61:103086. doi:10.1016/j.probenmech.2020.103086.
- [19] Meucci A. Review of Statistical Arbitrage, Cointegration, and Multivariate Ornstein-Uhlenbeck. *SSRN Electronic Journal*. 2009;doi:10.2139/ssrn.1404905.
- [20] Vatiwutipong P, Phewchean N. Alternative way to derive the distribution of the multivariate Ornstein-Uhlenbeck process. *Advances in Difference Equations*. 2019;2019(1):276. doi:10.1186/s13662-019-2214-1.
- [21] Eaton ML. *Multivariate Statistics: A Vector Space Approach*. Lecture notes-monograph series. 2007;53:i–512.
- [22] Robbins H. A remark on Stirling’s formula. *The American Mathematical Monthly*. 1955;62(1):26–29. doi:10.2307/2308012.
- [23] Mehr CB, McFadden JA. Certain properties of Gaussian processes and their first-passage times. *Journal of the Royal Statistical Society: Series B (Methodological)*. 1965;27(3):505–522. doi:10.1111/j.2517-6161.1965.tb00611.x.
- [24] Ricciardi LM, Sato S. First-passage-time density and moments of the Ornstein-Uhlenbeck process. *Journal of Applied Probability*. 1988;25(1):43–57. doi:10.2307/3214232.
- [25] Reeves GT. The engineering principles of combining a transcriptional incoherent feedforward loop with negative feedback. *Journal of Biological Engineering*. 2019;13(1):62. doi:10.1186/s13036-019-0190-3.
- [26] Khammash MH. Perfect adaptation in biology. *Cell Systems*. 2021;12(6):509–521. doi:10.1016/j.cels.2021.05.020.
- [27] Ghusinga KR, Dennehy JJ, Singh A. First-passage time approach to controlling noise in the timing of intracellular events. *Proceedings of the National Academy of Sciences*. 2017;114(4):693–698. doi:10.1073/pnas.1609012114.
- [28] Timm A, Yin J. Kinetics of virus production from single cells. *Virology*. 2012;424(1):11–17. doi:10.1016/j.virol.2011.12.005.

- [29] Jenner A, Yun CO, Yoon A, Kim PS, Coster ACF. Modelling heterogeneity in viral-tumour dynamics: The effects of gene-attenuation on viral characteristics. *Journal of Theoretical Biology*. 2018;454:41–52. doi:10.1016/j.jtbi.2018.05.030.

Supplementary material for
 “Smoothing in linear multicompartment biological processes
 subject to stochastic input”

Alexander P Browning¹, Adrienne L Jenner², Ruth E Baker¹, and Philip K Maini¹

¹*Mathematical Institute, University of Oxford, Oxford, United Kingdom*

²*School of Mathematical Sciences, Queensland University of Technology, Brisbane, Australia*

May 17, 2023

Contents

1 Derivation of smoothing results	2
1.1 Covariance matrix	3
1.1.1 Rescaled results	6
1.2 Autocorrelation function	6
1.2.1 Rescaled results	7
1.2.2 Expression in the general case	7
2 Vanishing covariance proof	9
3 Numerical solution to the Volterra equation	10

¹Corresponding author: browning@maths.ox.ac.uk

1 Derivation of smoothing results

In the main text, the unscaled system of equations is given by

$$\begin{aligned} dI &= -\theta(I - \mu) dt + \sigma dW, \\ dX_1 &= (I - kX_1) dt, \\ dX_\nu &= (kX_{\nu-1} - kX_\nu) dt, \quad \nu = 2, \dots, n, \end{aligned} \tag{1}$$

where $\theta, \mu, \sigma, k > 0$ are positive parameters. We introduce the scaled variables

$$\hat{X}_\nu = kX_\nu, \quad \hat{t} = kt, \tag{2}$$

such that

$$\begin{aligned} dI &= -\hat{\theta}(I - \mu) d\hat{t} + \hat{\sigma} dW, \\ d\hat{X}_1 &= (I - \hat{X}_1) d\hat{t}, \\ d\hat{X}_\nu &= (\hat{X}_{\nu-1} - \hat{X}_\nu) d\hat{t}, \quad \nu = 2, \dots, n, \end{aligned} \tag{3}$$

and where $\hat{\theta} = \theta/k$, $\hat{\sigma} = \sigma/\sqrt{k}$. Thus, we have the equivalent matrix system

$$d\hat{\mathbf{X}} = -\hat{\Theta}(\mathbf{X}(t) - \boldsymbol{\mu}) d\hat{t} + \hat{\mathbf{S}} d\mathbf{W}, \tag{4}$$

with

$$\hat{\Theta} = \begin{pmatrix} \hat{\theta} & 0 & 0 & 0 & \dots & 0 \\ -1 & 1 & 0 & 0 & \dots & 0 \\ 0 & -1 & 1 & 0 & \dots & 0 \\ & \vdots & & & \ddots & \\ 0 & 0 & 0 & 0 & \dots & 1 \end{pmatrix}, \quad \boldsymbol{\mu} = \mu \begin{pmatrix} 1 \\ \mathbf{\Theta}_{22}^{-1} \mathbf{e}_1 \end{pmatrix}, \quad \mathbf{S} = \begin{pmatrix} \hat{\sigma} & \mathbf{0} \\ \mathbf{0} & \mathbf{0} \end{pmatrix}. \tag{5}$$

In this section of the supporting material, we detail how we formulate expressions for the covariance and autocorrelation of the scaled process and, by extension, the results for the

unscaled process that are presented in the main document.

1.1 Covariance matrix

The stationary covariance matrix of the scaled process is given by

$$\text{vec}(\hat{\Sigma}_\infty) = \hat{\sigma}^2(\hat{\Theta} \oplus \hat{\Theta})^{-1}\mathbf{e}_1, \quad (6)$$

so we wish to find the first column of $(\hat{\Theta} \oplus \hat{\Theta})^{-1}$. Without loss of generality, we set $\hat{\sigma} = 1$ and rescale by the appropriate amount at the end.

The Kronecker sum is given by

$$\hat{\Theta} \oplus \hat{\Theta} = \begin{pmatrix} \mathbf{A} & \mathbf{0} & \mathbf{0} & \dots & \mathbf{0} \\ -\mathbf{I} & \mathbf{B} & \mathbf{0} & \dots & \mathbf{0} \\ \mathbf{0} & -\mathbf{I} & \mathbf{B} & \dots & \mathbf{0} \\ \vdots & & & \ddots & \\ \mathbf{0} & \mathbf{0} & \mathbf{0} & \dots & \mathbf{B} \end{pmatrix}, \quad (7)$$

with

$$\mathbf{A} = \begin{pmatrix} 2\hat{\theta} & 0 & 0 & \dots & 0 \\ -1 & 1 + \hat{\theta} & 0 & \dots & 0 \\ 0 & -1 & 1 + \hat{\theta} & \dots & 0 \\ \vdots & & & \ddots & \\ 0 & 0 & 0 & \dots & 1 + \hat{\theta} \end{pmatrix}, \quad \mathbf{B} = \begin{pmatrix} 1 + \hat{\theta} & 0 & 0 & \dots & 0 \\ -1 & 2 & 0 & \dots & 0 \\ 0 & -1 & 2 & \dots & 0 \\ \vdots & & & \ddots & \\ 0 & 0 & 0 & \dots & 2 \end{pmatrix}. \quad (8)$$

The $\text{vec}(\cdot)$ forms a vector by stacking the columns of a matrix argument. Therefore, the entries in the block-lower-diagonal of eq. (7) refer simply to the entries in the preceding row (or column, given the covariance matrix is symmetric) of the covariance matrix. It is trivial to solve for the first n elements of $(\hat{\Theta} \oplus \hat{\Theta})^{-1}$ using back substitution, corresponding to the first row and column of the covariance matrix, yielding the recurrence relation

$$\hat{\Sigma}_\infty^{(1,1)} = \frac{1}{2\hat{\theta}}, \quad \hat{\Sigma}_\infty^{(1,j)} = \frac{\hat{\Sigma}_\infty^{(1,j-1)}}{1 + \hat{\theta}}, \quad j = 2, 3, \dots, \quad (9)$$

with solution

$$\hat{\Sigma}_\infty^{(1,j)} = \frac{1}{2\hat{\theta}(1 + \hat{\theta})^{j-1}}, \quad j = 2, 3, \dots \quad (10)$$

Applying back substitution to the remaining rows and columns yields the recurrence relation for the remaining elements

$$\hat{\Sigma}_\infty^{(i,j)} = \frac{\hat{\Sigma}_\infty^{(i,j-1)} + \hat{\Sigma}_\infty^{(i-1,j)}}{2}, \quad i, j = 2, 3, \dots \quad (11)$$

While beyond the scope of the present work, a more general recurrence relation can be derived where the transfer rates vary throughout the system. In this case, the recurrence relation

satisfied by elements of the covariance matrix is of the form

$$\begin{aligned}\hat{\Sigma}_{\infty}^{(1,1)} &= \frac{1}{2\theta}, \\ \hat{\Sigma}_{\infty}^{(1,i)} &= \frac{k_{i-1}}{\theta + k_i} \hat{\Sigma}_{\infty}^{(1,i-1)} = \frac{\prod_{p=1}^{i-1} k_p}{2\theta \prod_{p=2}^i (\theta + k_p)}, \\ \hat{\Sigma}_{\infty}^{(i,j)} &= \frac{k_{i-1} \hat{\Sigma}_{\infty}^{(i-1,j)} + k_{j-1} \hat{\Sigma}_{\infty}^{(i,j-1)}}{k_i + k_j}.\end{aligned}$$

For $\hat{\theta} = 1$ (i.e., $\theta = k$), this yields the solution

$$\hat{\Sigma}_{\infty}^{(i,j)} = \frac{\Gamma(i+j-1)}{2^{i+j-1} \Gamma(i) \Gamma(j)}. \quad (12)$$

For the general case, the solution can be verified as

$$\begin{aligned}\hat{\Sigma}_{1,1} &= \frac{1}{2\theta}, \\ \hat{\Sigma}_{i,j} &= \sum_{p=1}^{j-1} \binom{i+p-3}{p-1} \frac{1}{2^{i+p-1} \hat{\theta} (1 + \hat{\theta})^{j-p}} + \sum_{p=1}^{i-1} \binom{j+p-3}{p-1} \frac{1}{2^{j+p-1} \hat{\theta} (1 + \hat{\theta})^{i-p}}.\end{aligned}$$

To verify the solution to the recurrence relation, consider that

$$\begin{aligned}\frac{\hat{\Sigma}_{i-1,j} + \hat{\Sigma}_{i,j-1}}{2} &= \underbrace{\sum_{p=1}^{j-1} \binom{i+p-4}{p-1} \frac{1}{2^{i+p-1} \hat{\theta} (1 + \hat{\theta})^{j-p}}}_{S_1} + \underbrace{\sum_{p=1}^{i-2} \binom{j+p-3}{p-1} \frac{1}{2^{j+p} \hat{\theta} (1 + \hat{\theta})^{i-p-1}}}_{S_2} \\ &+ \underbrace{\sum_{p=1}^{j-2} \binom{i+p-3}{p-1} \frac{1}{2^{i+p} \hat{\theta} (1 + \hat{\theta})^{j-p-1}}}_{S_3} + \underbrace{\sum_{p=1}^{i-1} \binom{j+p-4}{p-1} \frac{1}{2^{j+p-1} \hat{\theta} (1 + \hat{\theta})^{i-p}}}_{S_4},\end{aligned}$$

and consider the first summation

$$\begin{aligned}
S_1 &= \sum_{p=1}^{j-1} \binom{i+p-4}{p-1} \frac{1}{2^{i+p-1} \hat{\theta} (1+\hat{\theta})^{j-p}} \\
&= \frac{1}{2^i \hat{\theta} (1+\hat{\theta})^{j-1}} + \sum_{p=2}^{j-1} \binom{i+p-4}{p-1} \frac{1}{2^{i+p-1} \hat{\theta} (1+\hat{\theta})^{j-p}} \\
&= \frac{1}{2^i \hat{\theta} (1+\hat{\theta})^{j-1}} + \sum_{p=2}^{j-1} \left\{ \binom{i+p-3}{p-1} - \binom{i+p-4}{p-2} \right\} \frac{1}{2^{i+p-1} \hat{\theta} (1+\hat{\theta})^{j-p}} \\
&= \frac{1}{2^i \hat{\theta} (1+\hat{\theta})^{j-1}} + \sum_{p=2}^{j-1} \binom{i+p-3}{p-1} \frac{1}{2^{i+p-1} \hat{\theta} (1+\hat{\theta})^{j-p}} - \sum_{p=2}^{j-1} \binom{i+p-4}{p-2} \frac{1}{2^{i+p-1} \hat{\theta} (1+\hat{\theta})^{j-p}} \\
&= \frac{1}{2^i \hat{\theta} (1+\hat{\theta})^{j-1}} + \underbrace{\sum_{p=1}^{j-1} \binom{i+p-3}{p-1} \frac{1}{2^{i+p-1} \hat{\theta} (1+\hat{\theta})^{j-p}}}_{T_1} - \frac{1}{2^i \hat{\theta} (1+\hat{\theta})^{j-1}} - \sum_{p=2}^{j-1} \binom{i+p-4}{p-2} \frac{1}{2^{i+p-1} \hat{\theta} (1+\hat{\theta})^{j-p}} \\
&= T_1 - \sum_{p=1}^{j-2} \binom{i+p-3}{p-1} \frac{1}{2^{i+p} \hat{\theta} (1+\hat{\theta})^{j-p-1}}.
\end{aligned}$$

Noting that the remainder term above is equal to S_3 , we have that

$$S_1 + S_3 = T_1 = \sum_{p=1}^{j-1} \binom{i+p-3}{p-1} \frac{1}{2^{i+p-1} \hat{\theta} (1+\hat{\theta})^{j-p}}.$$

Similarly, it can be shown that

$$S_2 + S_4 = T_2 = \sum_{p=1}^{i-1} \binom{j+p-3}{p-1} \frac{1}{2^{j+p-1} \hat{\theta} (1+\hat{\theta})^{i-p}},$$

such that

$$\frac{\hat{\Sigma}_{i-1,j} + \hat{\Sigma}_{i,j-1}}{2} = \sum_{i=1}^4 S_i = \hat{\Sigma}_{i,j},$$

as required.

For $i = j = \nu - 1$, the scaled variance of the ν th compartment is given by

$$\begin{aligned}
\hat{\sigma}_\nu^2 &= \hat{\Sigma}_{\nu+1, \nu+1} = 2 \sum_{p=1}^{\nu} \binom{\nu+p-2}{p-1} \frac{1}{2^{\nu+p} \hat{\theta} (1+\hat{\theta})^{\nu-p+1}} \\
&= \frac{2^{1-\nu}}{\hat{\theta} (1+\hat{\theta})^{\nu+1}} \sum_{p=1}^{\nu} \binom{\nu+p-2}{p-1} \left(\frac{1+\hat{\theta}}{2} \right)^p \\
&= \frac{2^{1-\nu}}{\hat{\theta} (1+\hat{\theta})^{\nu+1}} \sum_{p=0}^{\nu-1} \binom{\nu+p-1}{p} \left(\frac{1+\hat{\theta}}{2} \right)^{p+1} \\
&= \frac{1}{\hat{\theta} (1-\hat{\theta}^2)^\nu} \sum_{p=0}^{\nu-1} \binom{\nu+p-1}{p} \left(\frac{1+\hat{\theta}}{2} \right)^p \left(\frac{1-\hat{\theta}}{2} \right)^\nu \\
&= \frac{1}{\hat{\theta} (1-\hat{\theta}^2)^\nu} \frac{\text{B}\left(\frac{1-\hat{\theta}}{2}, \nu, \nu\right)}{\text{B}(\nu, \nu)},
\end{aligned}$$

where we have exploited the similarity with the summand and the probability mass function of the negative binomial distribution [1].

1.1.1 Rescaled results

To obtain rescaled results we note that

$$\text{cov}(I, X_\nu) = \text{cov}\left(I, \frac{\hat{X}_\nu}{k}\right) = \frac{\text{cov}(I, \hat{X}_\nu)}{k},$$

and that

$$\text{cov}(X_{\nu_1}, X_{\nu_2}) = \text{cov}\left(\frac{\hat{X}_{\nu_1}}{k}, \frac{\hat{X}_{\nu_2}}{k}\right) = \frac{\text{cov}(\hat{X}_{\nu_1}, \hat{X}_{\nu_2})}{k^2}. \quad (13)$$

1.2 Autocorrelation function

We require $\text{cov}(\hat{X}_\nu(\hat{s}), \hat{X}_\nu(\hat{t}))$ where $\hat{t} = \hat{s} + \hat{\ell}$ and $\hat{s}, \hat{t} \gg 1$. We therefore require the final element of the matrix product

$$e^{-\hat{\Theta} \hat{\ell}} \hat{\Sigma}_\infty. \quad (14)$$

In the case that $\hat{\theta} = 1$ (i.e., $\theta = k$), we can write

$$-\hat{\Theta} = \mathbf{L} - \mathbf{I}, \quad (15)$$

where \mathbf{L} is a matrix comprising only 1 on the lower-diagonal (all other elements are zero), and \mathbf{I} is an identity matrix. Since \mathbf{I}_θ and \mathbf{L} commute, we have that

$$e^{-\hat{\Theta} \hat{\ell}} = e^{\mathbf{L} \hat{\ell} - \mathbf{I} \hat{\ell}} = e^{\mathbf{L} \hat{\ell}} e^{-\mathbf{I} \hat{\ell}} \in \mathbb{R}^{n \times n}, \quad (16)$$

where $n = \nu + 1$. The second factor, $e^{-\mathbf{I} \hat{\ell}} = e^{-\hat{\ell} \mathbf{I}}$ is trivial to compute. To compute $e^{\mathbf{L} \hat{\ell}}$

(specifically, we are only interested in the last row), we note that

$$\mathbf{L}^n = \mathbf{0}. \quad (17)$$

Therefore,

$$\mathbf{e}^{\mathbf{L}\hat{\ell}} = \sum_{i=0}^{n-1} \frac{\hat{\ell}^i}{i!} \mathbf{L}^i. \quad (18)$$

Furthermore, we note that raising \mathbf{L} to successive powers has the effect of shifting the diagonal downwards. Therefore, the only non-zero element of the last row of \mathbf{L}^i is element $n - i$ for $0 \leq i \leq n$. This yields the elements of the last row of $\mathbf{e}^{\mathbf{L}\hat{\ell}}$ as

$$[\mathbf{e}^{-\Theta\hat{\ell}}]_{n,i} = \frac{\hat{\ell}^{n-i}}{(n-i)!}. \quad (19)$$

Thus, the autocovariance is given by

$$\text{cov}(\hat{X}_\nu(\hat{s}), \hat{X}_\nu(\hat{t})) = e^{-\hat{\ell}} \sum_{i=1}^n \frac{\hat{\ell}^{n-i} \hat{\Sigma}_\infty^{(i,n)}}{\Gamma(n-i+1)}. \quad (20)$$

The expression for the autocorrelation function of the ν th compartment can be further simplified through the use of hypergeometric functions

$$\hat{\rho}_\nu(\hat{\ell}) = \frac{e^{-\hat{\ell}}}{\hat{\sigma}_\nu^2} \sum_{i=1}^{\nu+1} \frac{\hat{\Sigma}_\infty^{(\nu-i+2, \nu+1)} \hat{\ell}^{i-1}}{\Gamma(i)} \quad (21)$$

$$= e^{-\hat{\ell}} {}_1F_1(-\nu, -2\nu, 2\hat{\ell}) \quad (22)$$

$$= e^{-\hat{\ell}} \left(1 + \hat{\ell} + \mathcal{O}(\hat{\ell}^2)\right). \quad \nu \geq 2. \quad (23)$$

An exact expression for the second derivative at $\hat{\ell} = 0$ can be calculated as

$$\hat{\rho}_\nu''(0) = \frac{1}{1-2\nu}.$$

1.2.1 Rescaled results

To obtain the rescaled results we note that correlations are insensitive to scaling. Thus,

$$\rho_\nu(\ell) = \hat{\rho}_\nu(k\ell),$$

with the second derivative then given by

$$\rho_\nu''(0) = \frac{k^2}{1-2\nu}.$$

1.2.2 Expression in the general case

While not trivial and beyond the scope of the present work, an expression for the autocorrelation function can also be derived in the general case. We conjecture based on expressions for systems

with $n \leq 6$ that the scaled autocorrelation function is given in the general case by

$$\hat{\rho}_\nu(\hat{\ell}) = \frac{1}{\hat{\sigma}_\nu^2} \left\{ \hat{\Sigma}_\infty^{(1, \nu+1)} \left(\frac{(-1)^\nu e^{-\hat{\theta}\hat{\ell}}}{(\hat{\theta}-1)^\nu} + \sum_{i=1}^{\nu} \frac{(-1)^{i+1} e^{-\hat{\ell}\hat{\ell}^{\nu-i}}}{\Gamma(\nu-i+1)(\hat{\theta}-1)^i} \right) + \sum_{i=2}^{\nu+1} \frac{\hat{\Sigma}_\infty^{(i, \nu+1)} e^{-\hat{\ell}\hat{\ell}^{\nu-i+1}}}{\Gamma(\nu-i+2)} \right\}.$$

2 Vanishing covariance proof

Proposition 1. *Let $i, j \in \mathbb{Z}^+$ such that $i < j$ and let $\theta > 0$. If $j > i$, then $\hat{\Sigma}_\infty^{(i,j)} < \hat{\Sigma}_\infty^{(i,j-1)}$. Further, if $i > 1$, we additionally have that $\hat{\Sigma}_\infty^{(i-1,j)} < \hat{\Sigma}_\infty^{(i,j)}$.*

Proof. (By induction) Since $\hat{\Sigma}_\infty^{(1,i)} = \hat{\Sigma}_\infty^{(1,i-1)}/(1+\theta)$ and $\theta > 0$, we have that the statement is true for $i = 1$. For $i = 2$, consider first that $\hat{\Sigma}_\infty^{(2,2)} = \hat{\Sigma}_\infty^{(1,2)}$ where we have used the fact that $\hat{\Sigma}_\infty^{(i-1,i)} = \hat{\Sigma}_\infty^{(i,i-1)}$. Next, we have that $\hat{\Sigma}_\infty^{(2,3)} = \frac{1}{2} \left(\hat{\Sigma}_\infty^{(2,2)} + \hat{\Sigma}_\infty^{(1,3)} \right)$. Since $\hat{\Sigma}_\infty^{(1,3)} < \hat{\Sigma}_\infty^{(1,2)} = \hat{\Sigma}_\infty^{(2,2)}$, we have that $\hat{\Sigma}_\infty^{(1,3)} < \hat{\Sigma}_\infty^{(2,3)} < \hat{\Sigma}_\infty^{(2,2)}$ and so the statement is true for $j = i + 1$. Assuming that the statement holds for $j = k \geq i$, then $\hat{\Sigma}_\infty^{(i,k+1)} = \frac{1}{2} \left(\hat{\Sigma}_\infty^{(i,k)} + \hat{\Sigma}_\infty^{(i-1,k+1)} \right)$. Now, $\hat{\Sigma}_\infty^{(i-1,k)} < \hat{\Sigma}_\infty^{(i,k)} < \hat{\Sigma}_\infty^{(i,k-1)}$ and $\hat{\Sigma}_\infty^{(i-2,k+1)} < \hat{\Sigma}_\infty^{(i-1,k+1)} < \hat{\Sigma}_\infty^{(i-1,k)}$ and so $\hat{\Sigma}_\infty^{(i-1,k+1)} < \hat{\Sigma}_\infty^{(i,k)}$. Therefore, $\hat{\Sigma}_\infty^{(i-1,k+1)} < \hat{\Sigma}_\infty^{(i,k+1)} < \hat{\Sigma}_\infty^{(i,k)}$ and so by the principle of mathematical induction, the statement holds for $j \geq i = 2$. The inductive step can be repeated following the assumption that the statement is true for all $j \geq i = \ell$ to complete the proof. \square

Proposition 2. *For all $\nu \in \mathbb{N} \cup \{0\}$, $\sigma_{\nu+1}^2 < \sigma_\nu^2$.*

Proof. Given that as $\sigma_\nu^2 = \hat{\Sigma}_\infty^{(\nu+1,\nu+1)}$, we need to show that $\hat{\Sigma}_\infty^{(i+1,i+1)} < \hat{\Sigma}_\infty^{(i,i)}$ for $i \geq 2$. First, we note that $\hat{\Sigma}_\infty^{(i+1,i+1)} = \hat{\Sigma}_\infty^{(i,i+1)}$. From the previous proposition, we have that $\hat{\Sigma}_\infty^{(i-1,i+1)} < \hat{\Sigma}_\infty^{(i,i+1)} < \hat{\Sigma}_\infty^{(i,i)}$ and so $\hat{\Sigma}_\infty^{(i+1,i+1)} < \hat{\Sigma}_\infty^{(i,i)}$. \square

Corollary 1. *For $\theta > 0$, $\lim_{\nu \rightarrow \infty} \sigma_\nu^2 = 0$*

Proof. It suffices to note that

$$\lim_{j \rightarrow \infty} \hat{\Sigma}_\infty^{(1,j)} = \lim_{j \rightarrow \infty} \frac{1}{2\hat{\theta}(1+\hat{\theta})^{j-1}} = 0.$$

Similar logic to Proposition 1 can be applied to show that $\hat{\Sigma}_\infty^{(1,j)} \geq \hat{\Sigma}_\infty^{(j,j)}$, and so $\sigma_\nu^2 = \hat{\Sigma}_\infty^{(\nu+1,\nu+1)} \leq \hat{\Sigma}_\infty^{(1,\nu+1)}$, the latter of which vanishes as $\nu \rightarrow \infty$, thus σ_ν^2 also vanishes as $\nu \rightarrow \infty$. \square

3 Numerical solution to the Volterra equation

We solve the Volterra equation of the first kind

$$p(t) = \int_0^t K(s, t) f(s) ds, \quad (24)$$

numerically, using the midpoint rule and regularisation to find an approximate solution for $f(t)$ [2]. First, consider that the Volterra equation of the second kind

$$p(t) = \alpha_1 f(t) + \int_0^t K(s, t) f(s) ds, \quad (25)$$

is equivalent to eq. (24) for $\alpha_1 = 0$. We discretise the integral in eq. (25) using the midpoint rule, such that

$$p(t_n) = \alpha_1 f_n + \sum_{i=1}^{n-1} K(s_i, t_n) f_i \Delta_i, \quad (26)$$

where

$$s_i = \frac{t_i + t_{i+1}}{2} \quad \text{and} \quad \Delta_i = t_{i+1} - t_i,$$

and $f_i = f(t_i)$ is to be determined.

We create a grid $\{t_1, \dots, t_N\}$ with geometric spacing such that

$$t_N - t_{N-1} = \omega(t_2 - t_1),$$

where ω is a parameter to be chosen ($\omega = 1$ recovers linear spacing). Equation (26), therefore, gives a system of N linear equations in $\mathbf{f} = [f_1, \dots, f_N]^\top$ for $n = 1, 2, \dots, N$, such that

$$\mathbf{p} = \alpha_1 \mathbf{I} + \mathbf{A} \mathbf{f} = \mathbf{M} \mathbf{f}, \quad (27)$$

for $\mathbf{p} = [p(t_1), \dots, p(t_N)]^\top$.

In general, the linear system eq. (27) may be poorly conditioned. Thus, we solve the minimisation problem

$$\min \|\mathbf{M} \mathbf{f} - \mathbf{p}\|^2 + \alpha_2 \|\mathbf{f}\|^2, \quad (28)$$

where α_2 is a second regularisation parameter. The solution to eq. (27) is given by the solution to the system

$$(\mathbf{M}^\top \mathbf{M} + \alpha_2 \mathbf{I}) \mathbf{f} = \mathbf{M}^\top \mathbf{p}. \quad (29)$$

Code implementing our numerical solution to the Volterra equation is given on Github at <https://github.com/ap-browning/multicompartment/blob/main/results/volterra.jl>.

References

- [1] Rider PR. The negative binomial distribution and the incomplete beta function. *The American Mathematical Monthly*. 1962;69(4):302. doi:10.2307/2312952.
- [2] Lamm PK. A survey of regularization methods for first-kind Volterra equations. In: *Surveys on Solution Methods for Inverse Problems*. Vienna: Springer; 2000. p. 53–82.